

# Parameters of Warm Molecular Clouds from Methyl Acetylene Observations

A. V. Alakoz<sup>1</sup>, S. V. Kalenskii<sup>1</sup>, V. G. Promislov<sup>1</sup>, L. E. B. Johansson<sup>2</sup>, and A. Winnberg<sup>2</sup>

<sup>1</sup> Astro Space Center, Lebedev Physical Institute, ul. Profsoyuznaya 84/32, Moscow, 117997. Russia

<sup>2</sup> Onsala Space Observatory, S-439 92, Onsala, Sweden

Received / Accepted

**Abstract.** The results of a survey of 63 galactic star-forming regions in the  $6_K - 5_K$  and  $5_K - 4_K$  methyl acetylene lines at 102 and 85 GHz, respectively, are presented. Forty-three sources were detected at 102 GHz, and twenty-five at 85 GHz. Emission was detected towards molecular clouds with kinetic temperatures 20–60 K (so-called “warm clouds”). The  $\text{CH}_3\text{CCH}$  abundances in these clouds appeared to be about several units  $\times 10^{-9}$ . Five mapped sources were analyzed using the maximum entropy method. The sizes of the mapped clouds fall within the range between 0.1 and 1.7 pc, virial masses — between 90 — 6200  $M_\odot$ , and densities — between  $6 \times 10^4$  and  $6 \times 10^5 \text{ cm}^{-3}$ . The  $\text{CH}_3\text{CCH}$  sources spatially coincide with the CO and CS sources. Chemical evolution simulations showed that the typical methyl acetylene abundance in the observed clouds corresponds to an age of  $\approx 6 \times 10^4$  years.

## 1. INTRODUCTION

Massive stars are known to form in so-called “warm” molecular clouds (Olmí et al. 1996; Kalenskii et al. 1997), which have temperatures 30 – 50 K, masses from hundreds to thousands  $M_\odot$ , and sizes 0.1 – 3 pc. Therefore the exploration of such clouds is an important part of the exploration of star formation. Warm clouds have been fairly well studied in lines of CO, CS,  $\text{NH}_3$ ,  $\text{CH}_3\text{OH}$  and many other molecules. However, the CO, CS,  $\text{NH}_3$ , and  $\text{CH}_3\text{OH}$  emissions are strongly affected by the contribution from compact regions of hot gas (hot cores), where the abundances of these and some other molecules are enhanced by several orders of magnitude owing to grain mantle evaporation.

To eliminate the contribution from hot cores, one should observe warm clouds in lines of molecules that weakly emit in such regions. One of these molecules is methyl acetylene. Its abundance is not enhanced in the Orion Hot Core (Wang et al. 1993), and, probably, it is not enhanced in other hot cores as well. Since hot cores, which have sizes of approximately 0.05 pc, are much smaller than warm clouds, their contribution to the  $\text{CH}_3\text{CCH}$  emission is probably negligible.

The rotational lines of methyl acetylene are grouped in series of  $J_K - (J-1)_K$  lines with closely spaced frequencies. The lines from the same series can be observed simultaneously with the same receiver, making it possible to obtain

accurate ratios of their intensities. Methyl acetylene observations allow determinations of the gas kinetic temperature. Radiative transitions between different  $K$ -ladders are prohibited by the selection rule  $\Delta K = 0$ ; thus, the ratios of different  $K$ -ladders’ populations are determined by collisions and depend mostly on the gas kinetic temperature. Since methyl acetylene has a fairly small dipole moment, 0.78 D (Bauer et al. 1979), it is collisionally thermalized even at density  $\approx 10^4 \text{ cm}^{-3}$ . In addition, methyl acetylene lines appeared to be optically thin in the warm clouds that have been already observed (Wang et al. 1993). These properties allow us to assume local thermodynamic equilibrium (LTE) and utilize simple methods of analysis, for instance, rotational diagrams, which produce fairly accurate temperature estimates in this case. Simulations by Askne et al. (1984) showed that the methyl acetylene rotational temperatures are approximately equal to the gas kinetic temperatures.

## 2. OBSERVATIONS

The observations were carried out in May 1997<sup>1</sup> with the 20-m millimeter-wave radio telescope of the Onsala Space Observatory, Sweden. The frequency, line strength, and upper level energy for each observed transition are given in Table 1. Pointing accuracy was checked using observations of SiO masers and was no worse than 5". The observations were performed in the dual beam switching

Send offprint requests to: A.V. Alakoz, e-mail: rett@tanatos.asc.rssi.ru

<sup>1</sup> Sensitive observations of four sources, W 3(OH), Orion KL, W 51E1/E2, and DR 21(OH) were conducted in 2000

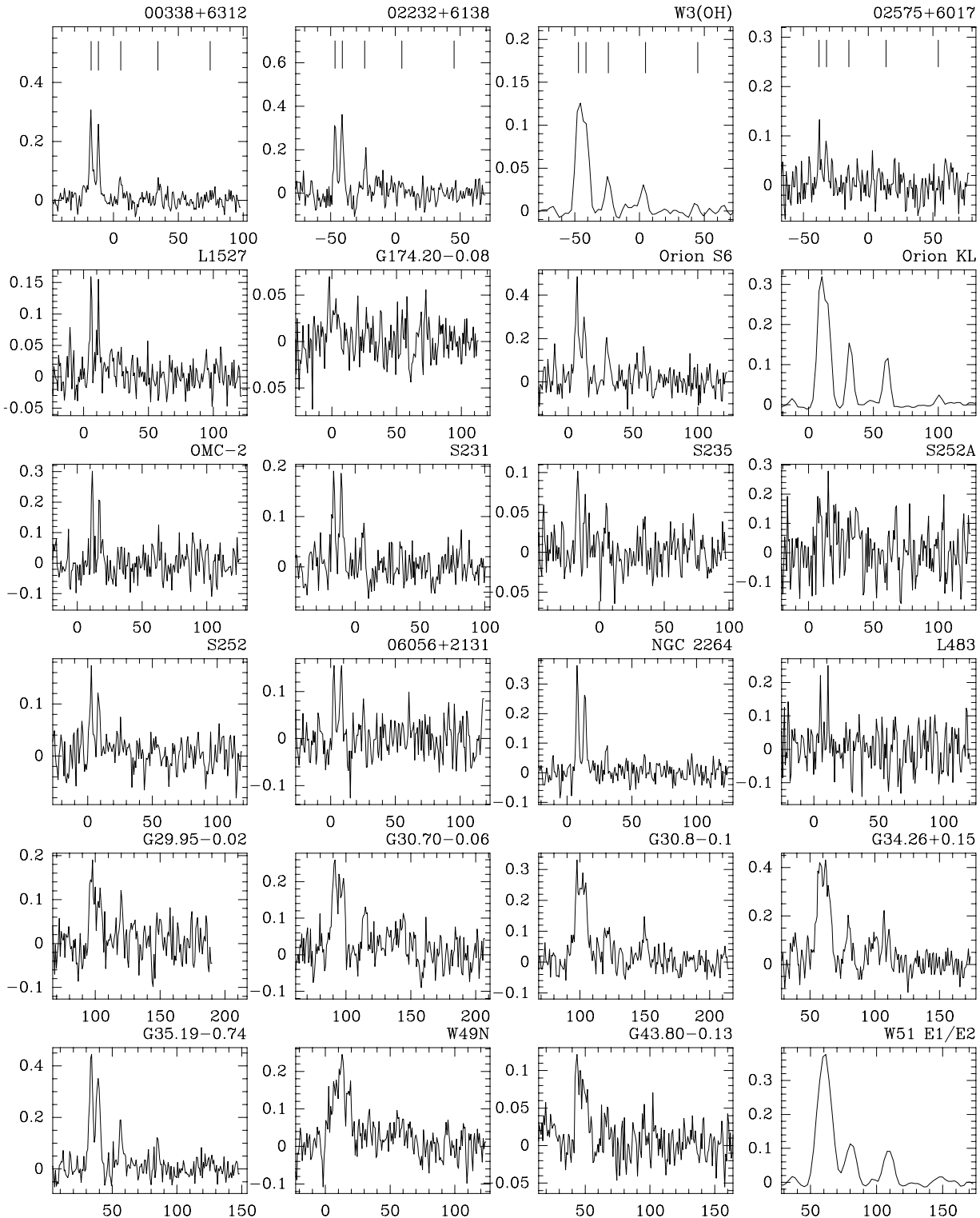


**Fig. 1.** Spectra of the sources detected in the  $6_K - 5_K$  lines. X-axis plots the LSR velocity of the  $6_0 - 5_0$  line in km/s; Y-axis plots the antenna temperature in Kelvins. The vertical lines in the upper row indicate the positions of different  $K$  components ( $K$  values increase to the right from 0 to 4).

mode with a beam separation of  $11'$  and a switch frequency of 2 Hz. The main-beam efficiency and full-width at half power were 0.55 and  $38''$ , respectively, at 102 GHz, and 0.6 and  $43''$  at 85 GHz. A cooled low-noise SiS mixer was used for the observations at both frequencies. The

system noise temperature, corrected for atmospheric absorption, rearward spillover, and radome losses, varied between 350 and 2000 K, depending on the weather conditions and source elevation. The data were calibrated using the chopper-wheel method. The backend consisted of two

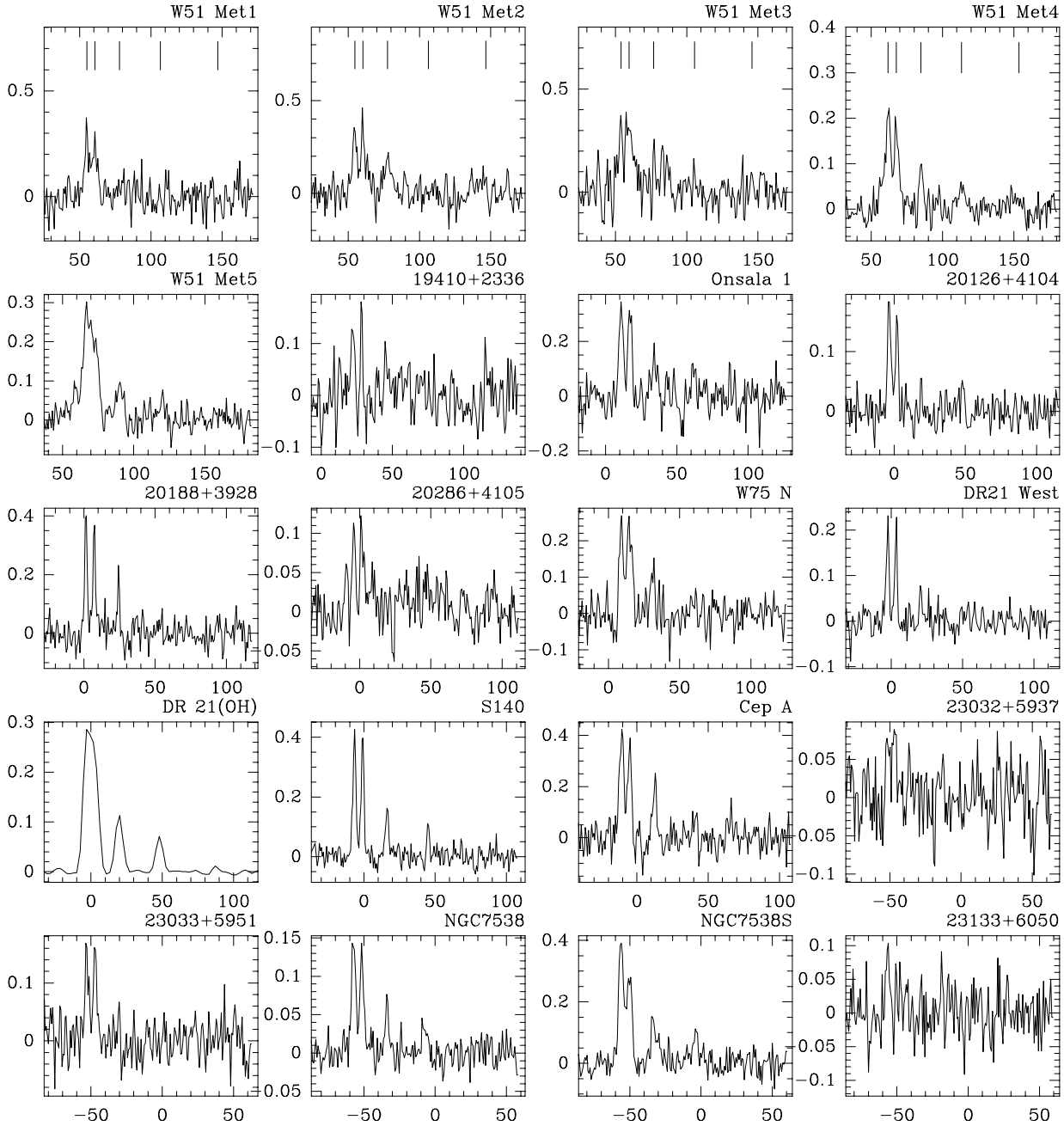


**Fig. 2.** Spectra of the sources detected in the  $6_K - 5_K$  lines (continued)

parallel filter spectrometers: a 256-channel spectrometer with 250 kHz resolution and a 512-channel spectrometer with 1 MHz resolution. Sixty-three sources were observed at 102 GHz. Thirty-two of these were observed at 85 GHz. When fitting Gaussians to the lines, we assumed that different  $J_K - (J - 1)_K$  lines with the same  $J$  have identical radial velocities and widths. The five sources NGC 2264, G30.8-0.1, G34.26+0.15, DR 21(OH), and S140 were mapped at 102 GHz. The mapping technique is described below.

Forty-five sources were detected at 102 GHz and twenty-five — at 85 GHz. The source coordinates and Gaussian parameters of the detected lines are presented

in Table 2. The spectra of the detected sources are shown in Figs. 1, 2, and 3.

### 3. DATA ANALYSIS

The spectra in Figs. 1, 2, and 3 demonstrate that in most of the sources only the  $K = 0$ ,  $K = 1$ , and  $K = 2$  lines with low excitation energies (Table 1) were detected, the  $K = 0$  and 1 lines being usually blended. Sometimes the  $K = 3$  line can be distinguished from the noise. Only in the four sources, observed in 2000 with a high sensitivity, very weak  $K = 4$  lines were detected.

Figure 4 shows the  $6_K - 5_K$  methyl cyanide spectra of three sources, observed by Kalenskii et al. (2000) with

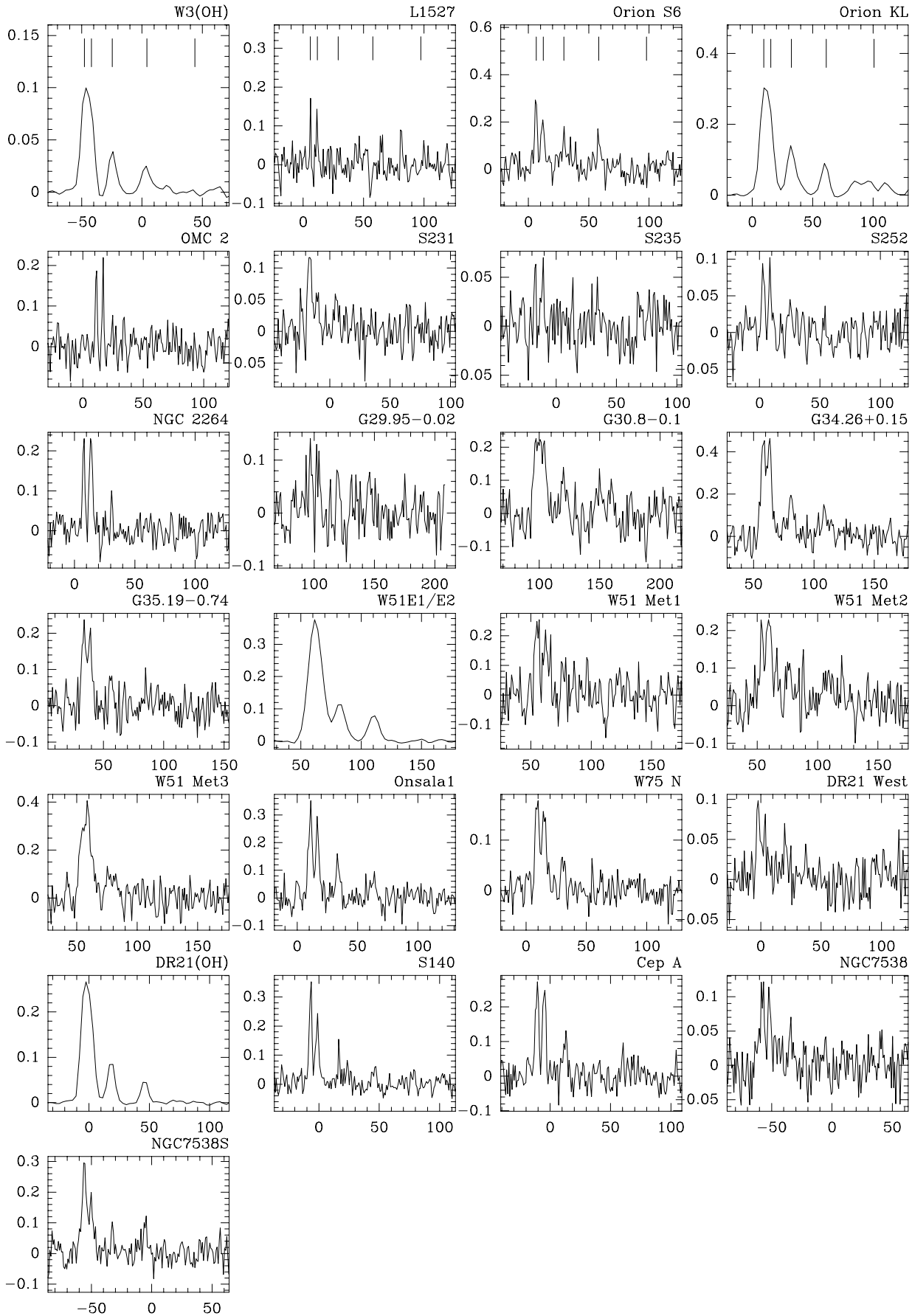


**Fig. 3.** Spectra of the sources detected in the  $5_K - 4_K$  lines. X-axis plots the LSR velocity of the  $5_0 - 4_0$  line in km/s; Y-axis plots the antenna temperature in Kelvins.

**Table 1.** Parameters of the observed methyl acetylene lines

Transition	Frequency (GHz)	S	$E_u/h$ (K)
6 <sub>0</sub> – 5 <sub>0</sub>	102547.984	6.00	12.315
6 <sub>1</sub> – 5 <sub>1</sub>	102546.024	5.83	19.300
6 <sub>2</sub> – 5 <sub>2</sub>	102540.144	5.33	40.258
6 <sub>3</sub> – 5 <sub>3</sub>	102530.348	4.50	75.181
6 <sub>4</sub> – 5 <sub>4</sub>	102516.573	3.33	124.060
6 <sub>5</sub> – 5 <sub>5</sub>	102499.110	1.83	186.885
5 <sub>0</sub> – 4 <sub>0</sub>	85457.272	5.00	8.209
5 <sub>1</sub> – 4 <sub>1</sub>	85455.622	4.80	15.196
5 <sub>2</sub> – 4 <sub>2</sub>	85450.730	4.20	36.153
5 <sub>3</sub> – 4 <sub>3</sub>	85442.528	3.20	71.076
5 <sub>4</sub> – 4 <sub>4</sub>	85431.224	1.80	119.956

the same equipment and with approximately the same sensitivity as the methyl acetylene lines. Methyl cyanide (CH<sub>3</sub>CN), like methyl acetylene, is a symmetric top molecule and its spectrum also consists of  $J_K - (J - 1)_K$  groups. The methyl acetylene and methyl cyanide spectra of NGC 7538S look alike (there are no lines with  $K > 3$  in both spectra) and the radial velocities are the same; therefore one can assume that the emission of both molecules arise in the same region. In W 3(OH) and G34.26+0.15, the contribution from hot cores to the methyl cyanide emission is significant (Kalenskii et al. 2000). In these objects, high energy lines are clearly detectable in the methyl cyanide spectra, but they are not noticeable in the methyl acetylene spectra. The high-energy CH<sub>3</sub>CN lines appear in the spectra of these sources due to the contribution from hot cores (Kalenskii et al. 2000), and the absence of detectable emission in analogous methyl acetylene lines suggests that the contribution from hot cores to the CH<sub>3</sub>CCH emission is insignificant. High-energy CH<sub>3</sub>CCH lines are either weak or not detected in all the observed sources. Since many of them harbor hot cores, it is reasonably to assume that the contribution from hot cores to the methyl acetylene emission is typically small.

We built rotational diagrams for 40 sources at 102 GHz and for 23 sources at 85 GHz (Fig. 6). The temperatures, derived from the rotational diagrams, fall in the range from 20 to 60 K, typical for warm clouds, and within errors agree with those derived from the observations of ammonia, methanol, and methyl cyanide (Kalenskii et al. 1997, 2000; Mauersberger et al. 1986; Churchwell et al. 1990; Molinari et al. 1996; Wouterloot et al. 1988; Wilson et al. 1990; Schreyer et al. 1996). Methyl acetylene column densities vary between  $4 \times 10^{13} \text{ cm}^{-2}$  and  $1.2 \times 10^{15} \text{ cm}^{-2}$ , in most of the sources being included in a much narrower range,  $1 - 5 \times 10^{14} \text{ cm}^{-2}$ .

The observations of W 3(OH), DR 21(OH), Orion KL, and W 51E1/E2, which resulted in a detection of a sufficient number of lines (up to  $K = 4$ ), were analysed not as-

suming that the lines are optically thin. We calculated the ratios of line brightness temperatures for different sets of gas temperatures and CH<sub>3</sub>CCH column densities assuming that the CH<sub>3</sub>CCH level populations are thermalized. The temperature varied between 10 and 200 K, column density — between  $10^{11}$  and  $10^{15} \text{ cm}^{-2}$ , the sources were assumed to be uniform. Then we selected the models that agreed with the observations according to the  $\chi^2$  criterion. The results are presented in Fig. 5, which shows that both optically thin models and models with the opacities  $\tau$  of the  $K = 0$  and 1 lines about unity may match the observations. In the latter case, the intensities of the lines proved to be approximately an order of magnitude higher than the observed intensities; hence, the models with  $\tau \approx 1$  are possible only if the CH<sub>3</sub>CCH emission is significantly diluted. Note that the gas temperatures, derived from the models with  $\tau \approx 1$  is only slightly lower than those derived from the rotational diagrams. Below we consider that the methyl acetylene lines are optically thin.

In the last column of Table 3 we present the methyl acetylene abundances  $N_{\text{CH}_3\text{CCH}}/N_{\text{H}_2}$ , which were determined employing <sup>13</sup>CO data (Kalenskii et al. 2000). The observations of the 1 – 0 <sup>13</sup>CO line at 110 GHz have also been performed at Onsala. The <sup>13</sup>CO and H<sub>2</sub> column densities were calculated assuming that the 1 – 0 <sup>13</sup>CO lines are optically thin, the gas temperatures are equal to the CH<sub>3</sub>CCH rotational temperatures, and the <sup>13</sup>CO abundance is equal to  $1.7 \times 10^{-6}$  (Lucas and Liszt 1998).

### 3.1. THE TECHNIQUE OF MAPPING

We mapped five methyl acetylene sources at 102 GHz: NGC 2264, G30.8-0.1, G34.26+0.15, DR 21(OH), and S 140. In each of them we observed 50 – 100 positions with 10 and 20 arcsec spacings in right ascension and declination. For each source we tried to expand the observed area until at the edges the emission vanishes, but due to the lack of time we could not observe sufficiently large areas towards G30.8 – 0.1 and DR 21(OH). Therefore both the maps of these sources and the source parameters, derived using the maps, are unreliable.

Since the beam was fairly large (about 40''), and the signal-to-noise ratio was often fairly low, the obtained images were heavily smoothed by the beam and distorted by the noise. Therefore we reconstructed the images with the method of maximum entropy.

The reconstruction of an image, distorted by the noise and smoothed by the beam is an incorrect problem, since high spatial frequencies are lost due to the limited spatial resolution, and there are no ways to restore them (in other words, an infinite number of "initial" images match the observed smooth image). The method of maximum entropy select from the multitude of acceptable images the one that has the maximal Shannon entropy

$$E(f) = - \sum_{i=1}^N f_i \log f_i \quad (1)$$

**Table 2.** Gaussian parameters for detected CH<sub>3</sub>CCH lines with 1 $\sigma$  errors. For each source the parameters of the 102 GHz lines are presented in the upper row, and those of the 85 GHz lines in the lower row.

Source	R.A. <sub>1950</sub>	K=0	$\int T_A^* dV$ (K·km s <sup>-1</sup> )				K=4	V <sub>LSR</sub> (km s <sup>-1</sup> )	FWHM (km s <sup>-1</sup> )
	DEC. <sub>1950</sub>		K=1	K=2	K=3				
00338+6312	00 33 53.3	0.81(0.05)	0.66(0.04)	0.22(0.04)	0.15(0.04)	<0.12	-17.33(0.06)	2.74(0.1)	
	63 12 33.0	not observed							
02232+6138	02 23 13.4	0.93(0.07)	1.06(0.08)	0.35(0.08)	<0.21	<0.21	-46.56(0.08)	2.79(0.1)	
	61 38 44.8	not observed							
W 3(OH)	02 23 17.3	0.74(0.02)	0.55(0.02)	0.24(0.02)	0.18(0.02)	0.04(0.02)	-47.097(0.09)	5.43(0.10)	
	61 38 58.0	0.64(0.02)	0.48(0.02)	0.28(0.01)	0.18(0.01)		-47.679(0.11)	6.74(0.12)	
02575+6017	02 57 35.6	0.21(0.04)	0.17(0.04)	<0.12	<0.12	<0.15	-37.96(0.15)	1.75(0.24)	
	60 17 22.6	not observed							
L 1527	04 36 49.3	0.22(0.03)	0.18(0.03)	<0.05			5.78(0.07)	1.21(0.10)	
	25 57 16.0	0.16(0.05)	0.19(0.07)	<0.09			5.97(0.08)	0.74(0.14)	
G174.20	05 27 32.2	0.16(0.04)	0.13(0.05)	<0.12			-2.39(0.35)	3.01(0.58)	
	33 45 52.0	not observed							
Orion S6	05 32 44.8	1.42(0.10)	0.95(0.09)	0.60(0.09)	<0.25		6.68(0.10)	3.22(0.13)	
	-5 26 00.0	0.66(0.09)	0.40(0.08)	0.44(0.08)	<0.24		6.48(0.11)	2.26(0.16)	
Orion KL	05 32 47.0	1.93(0.04)	1.46(0.04)	0.99(0.04)	0.79(0.04)	<0.13	9.13(0.06)	5.61(0.07)	
	-5 24 20.0	2.06(0.10)	1.41(0.10)	1.08(0.06)	0.70(0.06)		9.43(0.16)	7.53(0.18)	
OMC 2	05 32 59.9	0.53(0.07)	0.39(0.06)	<0.18			11.46(0.08)	1.47(0.11)	
	-5 11 29.0	0.34(0.05)	0.30(0.05)	<0.12			11.17(0.07)	1.31(0.11)	
S 231	05 35 51.3	0.45(0.05)	0.45(0.05)	0.20(0.05)	<0.15		-16.46(0.10)	2.43(0.15)	
	35 44 16.0	0.45(0.05)	0.18(0.05)	0.16(0.05)	<0.15		-16.56(0.21)	3.38(0.22)	
S 235	05 37 31.8	0.21(0.03)	0.11(0.03)	0.13(0.03)	<0.09		-16.90(0.13)	2.08(0.16)	
	35 40 18.0	0.14(0.03)	0.14(0.03)	<0.9					
S 252A	06 05 36.5	0.52(0.14)	0.47(0.14)	<0.18			8.77(0.33)	2.78(0.30)	
	20 39 34.0	not observed							
S 252	06 05 53.7	0.31(0.05)	0.25(0.05)	0.10(0.04)	<0.12	<0.12	2.74(0.13)	2.11(0.23)	
	21 39 09.0	0.29(0.04)	0.27(0.04)	<0.12			2.94(0.15)	2.78(0.21)	
06056+2131	06 05 41.0	0.40(0.06)	0.45(0.07)	0.18(0.06)	<0.15	<0.15	2.61(0.12)	2.21(0.21)	
	21 31 32.2	not observed							
NGC 2264	06 38 24.9	0.75(0.05)	0.63(0.05)	0.18(0.04)	<0.12		8.06(0.05)	2.10(0.08)	
	09 32 28.0	0.57(0.05)	0.68(0.05)	0.19(0.05)	<0.15		7.97(0.08)	2.47(0.11)	
L 483	18 14 50.6	0.22(0.07)	0.25(0.06)	<0.10	<0.10	<0.10	5.11(0.14)	0.96(0.12)	
	-04 40 49.0	not observed							
G29.95-0.02	18 43 27.1	0.71(0.08)	0.47(0.08)	0.31(0.08)	<0.21	<0.15	97.35(0.21)	3.78(0.21)	
	-02 42 36.0	0.44(0.08)	0.44(0.08)	0.30(0.07)	<0.21				
G30.70-0.06	18 44 58.9	1.15(0.09)	0.95(0.09)	0.44(0.08)	0.33(0.08)	<0.24	91.27(0.19)	4.53(0.19)	
	-02 04 27.0	not observed							
G30.8-0.1	18 45 11.0	1.43(0.08)	1.36(0.08)	0.58(0.08)	0.52(0.07)	<0.6	98.00(0.00)	5.35(0.20)	
	-01 57 57.0	1.49(0.15)	1.42(0.15)	0.85(0.14)	0.51(0.13)	<0.09	97.83(0.31)	6.01(0.37)	
G34.26+0.15	18 50 46.1	2.32(0.12)	2.42(0.12)	1.27(0.10)	0.49(0.10)	<0.3	57.64(0.15)	6.02(0.17)	
	01 11 12.0	2.26(0.12)	2.16(0.12)	1.03(0.11)	0.54(0.11)	<0.3	57.91(0.13)	4.75(0.15)	
G35.19-0.74	18 55 40.8	1.52(0.07)	1.30(0.07)	0.62(0.03)	0.34(0.04)	<0.18	33.61(0.01)	3.37(0.08)	
	01 36 30.0	0.98(0.09)	0.88(0.09)	0.43(0.08)	<0.24		33.63(0.01)	4.16(0.19)	
W 49N	19 07 49.9	0.79(0.88)	2.41(0.84)	0.73(0.14)	0.94(0.15)	<0.42	7.14(1.69)	13.49(0.77)	
	09 01 14.0	not observed							
G43.80-0.13	19 09 30.8	0.57(0.06)	0.44(0.05)	0.28(0.05)	<0.12	<0.12	44.41(0.28)	5.04(0.28)	
	09 30 47.0	not observed							
W 51E1/E2	19 21 26.2	2.70(0.19)	2.56(0.18)	1.49(0.07)	1.18(0.08)	0.23(0.07)	57.79(0.22)	9.93(0.16)	
	14 24 43.0	2.89(0.36)	2.16(0.34)	1.26(0.10)	0.97(0.10)		59.85(0.43)	10.73(0.26)	
W 51 MET1	19 21 26.2	1.17(0.13)	0.97(0.13)	<0.36	<0.27	<.27	55.03(0.22)	3.92(0.24)	
	14 23 32.0	1.31(0.15)	0.93(0.14)	<0.39					
W 51 MET2	19 21 28.8	1.52(0.14)	1.54(0.15)	0.98(0.15)	<0.39	<0.39	54.64(0.19)	4.36(0.27)	
	14 23 47.0	1.24(0.35)	1.15(0.30)	0.62(0.16)	0.64(0.10)	<0.21	55.53(0.87)	9.10(0.80)	
W 51 MET3	19 21 27.5	1.30(0.15)	1.50(0.15)	0.45(0.15)	<0.45		53.84(0.21)	3.50(0.00)	
	14 23 52.0	2.42(1.41)	1.41(1.49)	0.85(0.20)	<0.48		55.91(2.89)	7.88(1.15)	

**Table 2.** (Continued)

Source	R.A. <sub>1950</sub>	$\int T_A^* dV$ (K·km s <sup>-1</sup> )					$V_{LSR}$ (km·s <sup>-1</sup> )	FWHM (km·s <sup>-1</sup> )
	DEC. <sub>1950</sub>	K=0	K=1	K=2	K=3	K=4		
W 51 MET4	19 21 25.6	1.06(0.05)	0.81(0.05)	0.25(0.05)	0.30(0.05)	<0.15	61.77(0.12)	4.33(0.15)
	14 25 41.0	not observed						
W 51 MET5	19 21 20.5	2.25(0.05)	1.13(0.05)	0.75(0.05)	0.39(0.05)	<0.15	67.08(0.73)	9.34(0.73)
	14 24 12.0	not observed						
19410+2336	19 41 04.2	0.34(0.07)	0.34(0.05)	0.18(0.06)	<0.18	<0.18	22.55(0.13)	1.98(0.18)
	23 36 42.0	not observed						
Onsala 1	20 08 09.9	1.24(0.11)	1.18(0.10)	0.58(0.10)	0.39(0.10)	<0.27	11.17(0.12)	3.42(0.13)
	31 22 42.0	1.24(0.07)	0.98(0.07)	0.53(0.07)	0.31(0.07)	<0.21	11.05(0.09)	3.60(0.11)
20126+4104	20 12 40.96	0.55(0.03)	0.41(0.02)	0.15(0.02)	0.11(0.02)	<0.06	-3.64(0.04)	2.46(0.07)
	41 04 20.6	not observed						
20188+3928	20 18 50.6	1.02(0.09)	0.87(0.08)	0.43(0.08)	0.35(0.08)	<0.24	1.46(0.07)	2.11(0.12)
	39 28 18.6	not observed						
20286+4105	20 28 40.6	0.45(0.05)	0.45(0.05)	<0.15	<0.15	<0.15	-4.04(0.17)	3.36(0.20)
	41 05 38.1	not observed						
W 75N	20 36 50.4	0.96(0.08)	1.05(0.08)	0.44(0.08)	<0.24		9.03(0.13)	3.71(0.14)
	42 27 23.0	0.68(0.05)	0.60(0.05)	0.16(0.05)	<0.12		9.34(0.13)	3.67(0.13)
DR 21 West	20 37 07.6	0.50(0.04)	0.45(0.04)	0.16(0.03)	<0.12		-2.39(0.06)	2.04(0.09)
	42 08 46.0	0.32(0.05)	0.21(0.05)	0.14(0.04)	<0.12		-2.16(0.23)	3.21(0.33)
DR 21(OH)	20 37 13.8	1.72(0.02)	1.45(0.02)	0.72(0.01)	0.43(0.01)	0.06(0.01)	-3.00(0.03)	5.87(0.03)
	42 12 13.0	1.59(0.03)	1.30(0.03)	0.60(0.02)	0.32(0.02)	<0.22	-4.11(0.08)	6.46(0.08)
S 140	22 17 41.2	1.09(0.05)	1.07(0.05)	0.44(0.05)	0.16(0.05)	<0.15	-6.62(0.04)	2.46(0.06)
	63 03 43.0	1.00(0.06)	0.69(0.06)	0.29(0.05)	0.17(0.05)	<0.15	-6.74(0.07)	2.88(0.11)
Cep A	22 54 19.2	1.56(0.10)	1.26(0.10)	0.80(0.10)	0.34(0.09)	<0.27	-10.70(0.09)	3.35(0.11)
	61 45 47.0	0.89(0.07)	0.88(0.07)	0.43(0.07)	<0.21		-10.58(0.10)	3.19(0.11)
23032+5937	23 03 16.9	0.23(0.07)	0.29(0.07)	<0.18	<0.18	<0.18	-51.91(0.34)	2.99(0.43)
	59 37 38.9	not observed						
23033+5951	23 03 19.7	0.48(0.06)	0.49(0.06)	<0.20	<0.20	<0.20	-52.94(0.13)	2.83(0.19)
	59 51 55.0	not observed						
NGC 7538	23 11 36.6	0.55(0.03)	0.46(0.03)	0.21(0.03)	0.11(0.03)	<0.09	-57.19(0.08)	3.36(0.10)
	61 11 50.0	0.34(0.05)	0.24(0.05)	0.12(0.04)	<0.15		-57.53(0.18)	2.89(0.22)
NGC 7538S	23 11 36.1	1.73(0.07)	1.27(0.06)	0.60(0.06)	0.40(0.06)	<0.18	-55.99(0.10)	4.09(0.09)
	61 10 30.0	1.15(0.07)	0.67(0.07)	0.25(0.07)	0.32(0.07)	<0.20	-55.76(0.13)	3.50(0.00)
23133+6050	23 13 21.5	0.24(0.07)	0.12(0.05)	<0.15	<0.15	<0.15	-56.30(0.19)	1.90(0.39)
	60 50 45.6							

where  $f_i$  is the intensity of an element of the image. We used the variant of the method, described by Wilchek and Drapatz (1985), except the computational algorithm to solve the optimization problem. The evolutionary algorithm, employed here, is described by Promislov (1999). The latter algorithm is more expensive computationally than that from Wilchek and Drapatz (1985), but in the case of a poor signal-to-noise ratio or insufficient grid spacing this algorithm may converge even if the algorithm from Wilchek and Drapatz (1985) fails. Nevertheless, among the observed lines only the blends of the  $6_0 - 5_0$  and  $5_0 - 4_0$  lines have sufficiently high signal-to-noise ratios to make the mapping possible. We made the maps of the intensity integrated over all the channels, occupied by the blends.

The images are shown in Fig. 7.

The resolution of the maps was estimated as follows: at each point of a map, we subtracted the contribution from the source, convolved with the beam, leaving only noise.

Then we added the contribution from a point source with flux equal to the observed flux, located at the peak of the reconstructed image, and convolved with the beam. Finally, we applied the image reconstruction procedure to this map. The size of the obtained image was adopted as the map resolution. The resolution of all maps proved to be about 15 – 25 arcsec, being significantly less than the sizes of the sources. Therefore the angular diameters, presented in Table 4, represent the real sizes of the sources.

### 3.2. COMMENTS ON INDIVIDUAL SOURCES

**NGC 2264.** The peak of CH<sub>3</sub>CCH emission coincide with the IR source IRS1 (Sargent et al. 1984) and the continuum sources at 130 and 70  $\mu$ m (Schreyer et al. 1997). The CH<sub>3</sub>CCH source is slightly extended to the southwest from the peak, and approximately coincides with the CS, C<sup>18</sup>O, CO, and CH<sub>3</sub>OH sources (Schreyer et al. 1997), but in our map there is no second peak approximately 30'' southwest

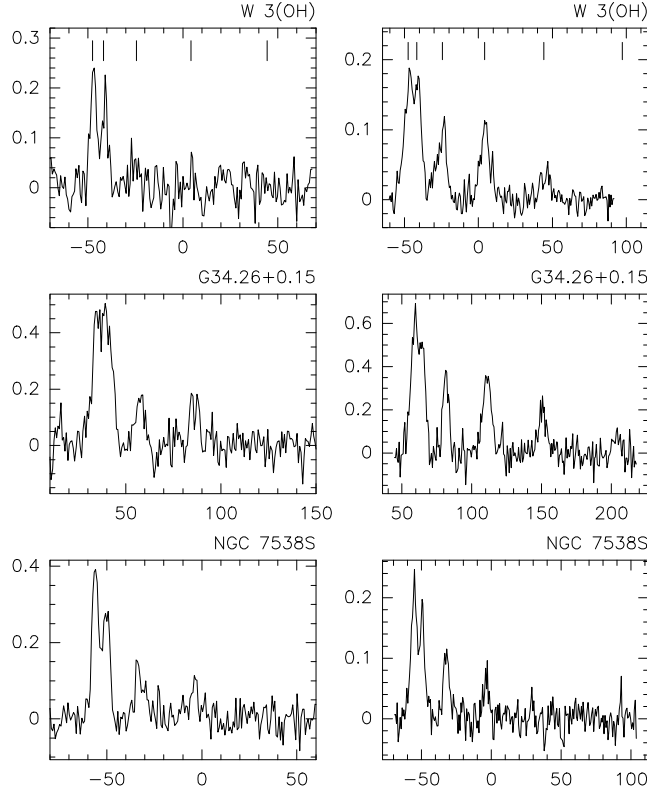


**Fig. 4.** Comparison of  $\text{CH}_3\text{CCH}$  and  $\text{CH}_3\text{CN}$  spectra (left and right columns, respectively).

from IRS1, which is present in the  $\text{C}^{18}\text{O}$ , CS, and  $\text{CH}_3\text{OH}$  maps.

**G34.26+0.15.** The  $\text{CH}_3\text{CCH}$  source is essentially circular with a diameter of  $50''$ . The peak of the emission coincides with an UC HII region (Benson and Johnston 1984) and the SO peak (Carral et al. 1987), but it is shifted approximately  $10''$  south-west from the  $\text{HCO}^+$  peak.

**DR 21(OH).** The methyl acetylene peak coincides with the continuum sources MM1 and MM2 (Padin et al. 1989) and the peaks of  $\text{H}_2\text{CO}$ ,  $\text{C}^{18}\text{O}$ , and CS emission (Johnston et al. 1989; Mangum et al. 1991). The methyl acetylene source is extended in the north-south direction by more than 2 arcmin, like the  $\text{C}^{18}\text{O}$  source (Padin et al. 1989). However, due to the lack of time we could not map the whole source, and the emission does not vanish at the northern edge of our map.

**S 140.** The source is slightly extended in the northeast-southwest direction; the peak of the emission coincides with the IR source IRS1 (Evans et al. 1989). Our map coincides fairly good with the  $^{12}\text{CO}$  maps (Snell et al. 1984; Minchin et al. 1993). At the same time, the peak of  $\text{CH}_3\text{CCH}$  emission is located 10–15 arcsec to the east from the  $^{13}\text{CO}$ ,  $\text{C}^{18}\text{O}$ , and  $\text{HCO}^+$  peaks (Minchin et al. 1995; Wilner and Welch 1994).

### 3.3. SOURCE PARAMETERS DERIVED FROM THE MAPS

We derived the virial masses of the mapped sources assuming that each source is a uniform optically thin nonmagnetized sphere of a constant density. According to Cesaroni et al. (1994), under these assumptions the virial mass can be calculated from the formula

$$M_{\text{vir}}(M_{\odot}) = 0.509 \cdot d \cdot \Theta_S \cdot \Delta v_{1/2}^2 \quad (2)$$

where  $\Theta_S$  is the source angular diameter in arcsec,  $\Delta v_{1/2}^2$  is the full-width at half maximum (FWHM) in  $\text{km s}^{-1}$ ,  $d$  is the source distance in kpc,  $M_{\text{vir}}(M_{\odot})$  is the cloud virial mass in  $M_{\odot}$ . The angular diameter of each source was estimated as follows: first, we calculated the map area (in  $\text{arcsec}^2$ ) within the contour that corresponds to the half-maximum intensity. This area was multiplied by  $\cos \delta$  to obtain the source area in the sky  $A$ . The angular diameter was calculated using the formula  $\Theta^2 = 4A/\pi$ , and additionally multiplied by 1.155 to obtain the sphere diameter from the visual diameter (Panagia and Walmsley 1978). The source distance was derived employing the Galactic rotation curve from Brand and Blitz (1993).

The masses, determined with Eq. (2), are presented in Table 4. In addition, we estimated the masses of the same sources using the  $^{13}\text{CO}$  column densities, assuming that the  $^{13}\text{CO}$  and  $\text{CH}_3\text{CCH}$  sources are spatially coinci-



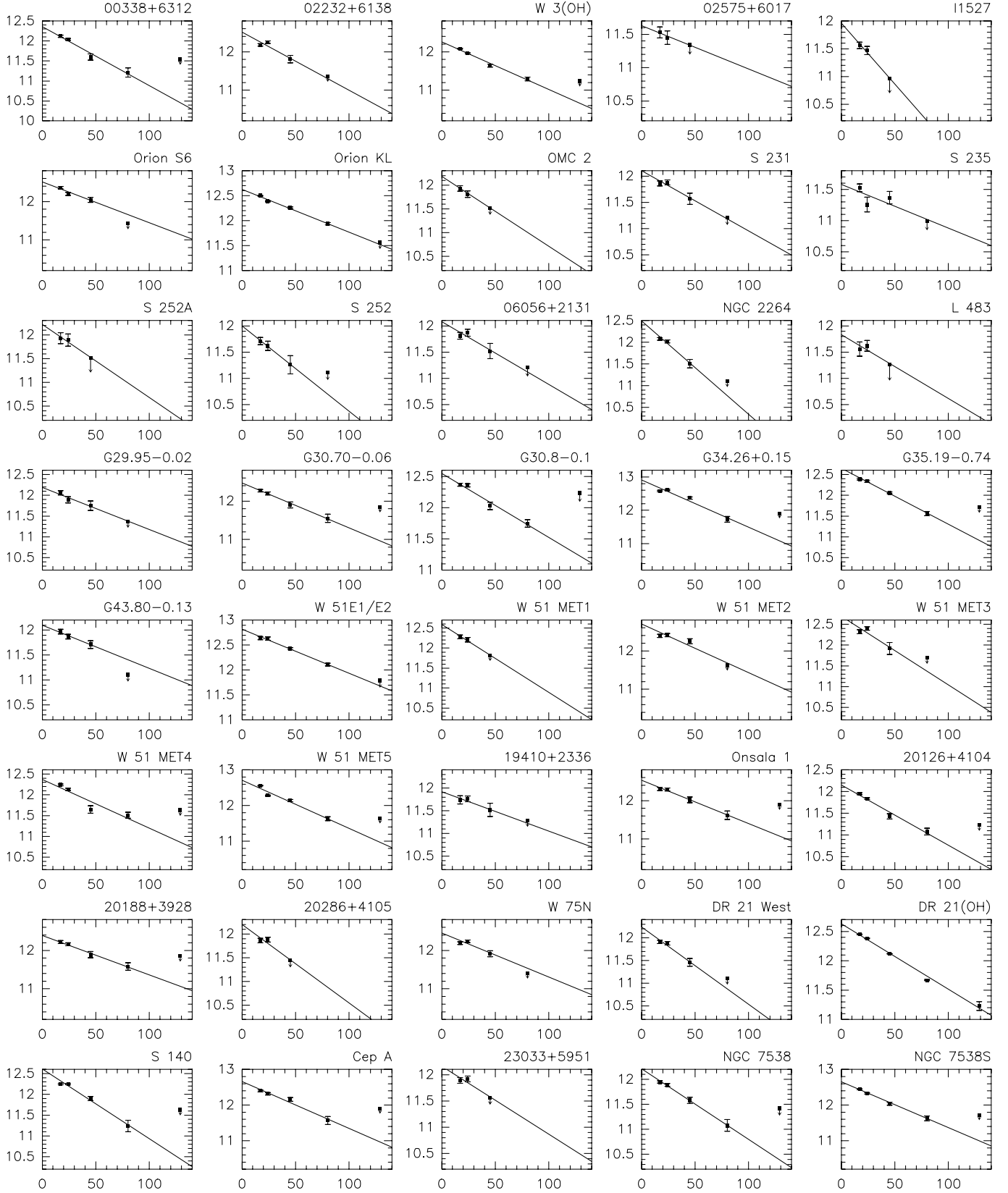


**Fig. 5.** Rotational diagrams for the  $6_K - 5_K$  lines. X-axis plots the upper level energies divided by the Boltzmann constant  $E_u/k$ , Y-axis plots the upper level populations divided by statistical weights  $\frac{\lg(3kW)}{8\pi^3\nu_0 S\mu_{ul}^2 g_l g_k}$  values. The arrows denote the upper level populations of undetected lines at  $3\sigma$  level.

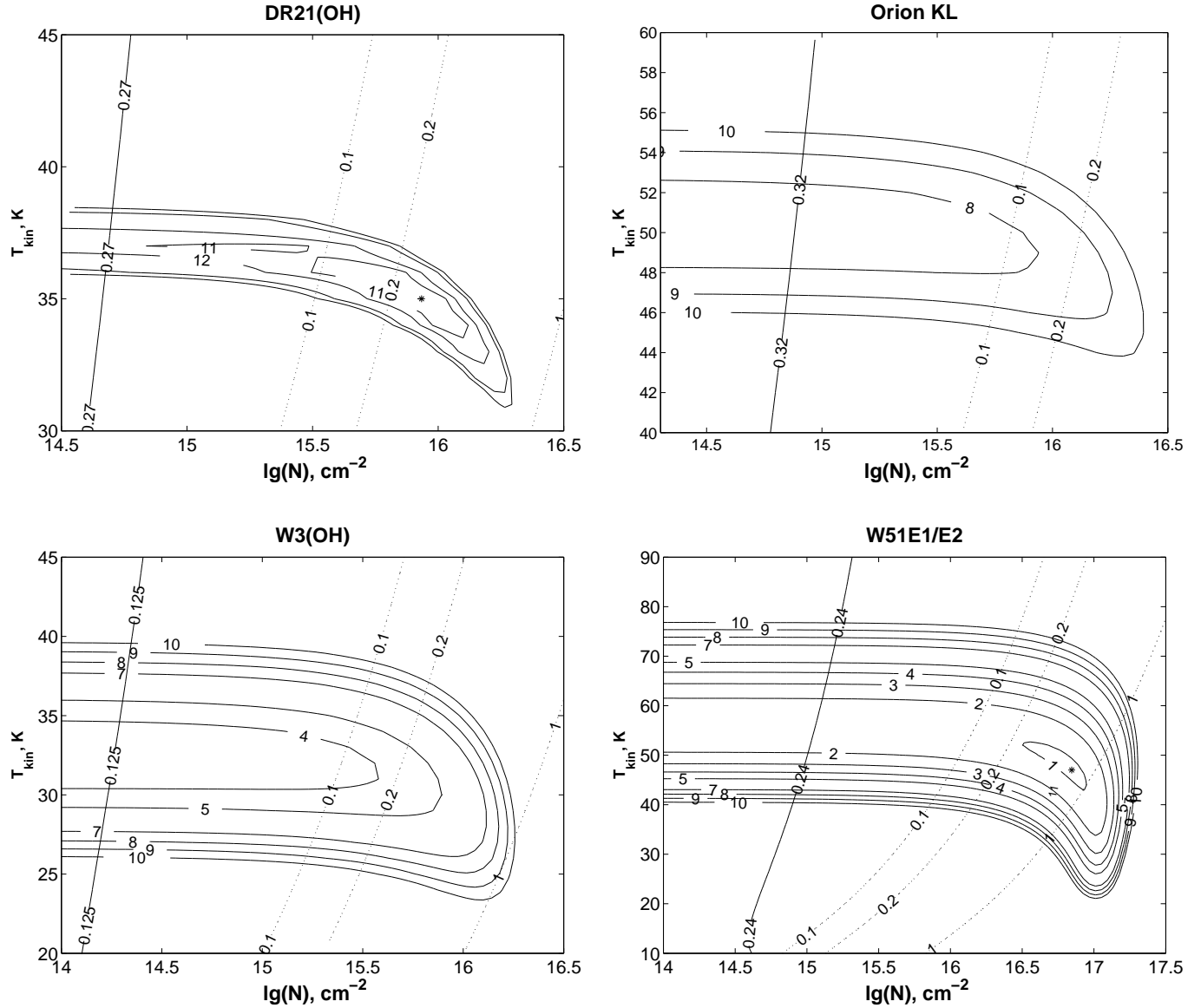


**Fig. 6.** Parameters of the sources determined by the  $\chi^2$  method. The contours show the derived  $\chi^2$  values, the oblique solid lines correspond to the parameter sets that produce the brightness temperature of the  $6_0 - 5_0$  line equal to the observed one. The dotted lines correspond to the parameter sets that provide the optical depths of the  $6_0 - 5_0$  line equal to 0.1, 0.2, and 1.

dent and the  $1-0$   $^{13}\text{CO}$  lines are optically thin. The latter masses are also presented in Table 4. For all sources, except G34.26+0.15, the virial masses coincide with the masses derived from  $^{13}\text{CO}$  column densities within a factor of two. The comparison of the intensities of the  $^{13}\text{CO}$  and  $\text{C}^{18}\text{O}$  lines in G34.26+0.15, presented in Little et al. (1994), leads to the conclusion that the  $^{13}\text{CO}$  lines are not optically thin. Hence, the derived  $^{13}\text{CO}$  column density and mass of this source are underestimated.

Since two different methods yield similar mass estimates of four sources, we believe that these estimates are correct.

Assuming that the masses of the sources are equal to their virial masses and using the source sizes and methyl acetylene column densities from Tables 3 and 4, we esti-

mated the gas densities and methyl acetylene abundances. The estimates are presented in Table 4. The densities appeared to be close to  $10^5 \text{ cm}^{-3}$ , and methyl acetylene abundances — of the order of several units  $\times 10^{-9}$ . So determined methyl acetylene abundances within a factor of two coincide with those presented in Table 3 in all sources except G34.26+0.15. We have already mentioned that the  $^{13}\text{CO}$  column density in this source is probably underestimated. In this case the methyl acetylene abundance, presented in Table 3, is overestimated, and the value of  $3.6 \times 10^{-9}$ , presented in Table 4, is more correct.

Our methyl acetylene abundances are in agreement with the abundances estimated for warm gas in Orion (Blake et al. 1987; Kuiper et al. 1984), Sgr B2 (Churchwell & Hollis 1983; Kuiper et al. 1984),

**Table 3.** Rotational temperatures and column densities determined from the methyl acetylene observations. The  $\text{CH}_3\text{CCH}$  abundances were derived from the column densities that were determined using the  $6_K - 5_K$  lines.

Source	102 GHz		85 GHz		$\text{CH}_3\text{CCH}$ abundance $\times 10^{-9}$
	$T_{rot}$ (K)	$N_{\text{CH}_3\text{CCH}}$ $\times 10^{14}$	$T_{rot}$ (K)	$N_{\text{CH}_3\text{CCH}}$ $\times 10^{14}$	
00338+6312	29 (1)	1.9 (0.2)			
02232+6138	29 (3)	2.6 (0.5)			
W 3(OH)	35 (0.7)	2.0 (0.1)	42.5 (2)	2.6 (0.2)	2.3
02575+6017	<67 (41)	<1.2 (1.2)			
L 1527	<20 (3)	<0.4 (0.1)			
ORI S6	41 (6)	4.4 (1.0)	<65 (22)	< 4.5 (2.3)	5.2
Orion KL	51 (1)	8.0 (0.3)	52 (4)	10.5 (1.3)	
OMC 2	<30 (6)	1.3 (0.4)	<34 (15)	< 1.1 (0.8)	4.1
S 231	38 (8)	1.5 (0.5)	29 (11)	1.1 (0.7)	4.8
S 235	<61 (11)	< 1.0 (0.3)			1.1
S 252A	<28 (10)	< 1.3 (0.9)			
S 252	27 (6)	0.7 (0.3)	<42 (22)	< 1.3 (1.0)	2.1
06056+2131	36 (10)	1.4 (0.6)			
NGC 2264	20 (1)	1.5 (0.2)	46 (20)	3.1 (2.0)	3.9
L483	<36 (20)	0.8 (0.7)			
G29.95-0.02	43 (10)	2.3 (0.9)	67 (25)	3.5 (2.1)	2.0
G30.70-0.06	37 (2)	3.5 (0.4)			
G30.8-0.1	42 (2)	5.1 (0.5)	50 (10)	8.2 (2.6)	5.7
G34.26+0.15	31 (1)	7.2 (0.5)	40 (4)	9.3 (1.7)	16
G35.19-0.74	32 (1)	4.3 (0.3)	44 (14)	4.4 (2.3)	8.5
G43.80-0.13	50 (13)	2.3 (1.0)			
W 51E1/E2	49 (3.5)	12 (1.5)	48 (5.5)	13.3 (2.7)	3.6
W 51 MET1	<26 (4)	< 2.8 (1.6)	<26 (9)	< 3.1 (1.7)	
W 51 MET2	<34 (2)	< 6.5 (2.2)	69 (19)	9.4 (4.6)	
W 51 MET3	26 (4)	3.5 (1.0)	34 (25)	7.4 (9.8)	2.5
W 51 MET4	37 (1)	2.8 (0.2)			
W 51 MET5	32 (0.5)	4.9 (0.2)			
19410+2336	40 (25)	1.5 (1.3)			
Onsala 1	39 (3)	4.2 (0.6)	39 (5)	4.7 (0.9)	6.1
20126+4104	31 (1)	1.3 (0.1)			
20188+3928	<42 (3)	< 3.6 (0.5)			
20286+4105	<26 (3.7)	< 1.1 (0.3)			
W 75N	38 (6)	3.4 (0.9)	29 (8)	1.9 (0.9)	24
DR 21 West	26 (3)	1.2 (0.2)	41 (19)	1.2 (0.9)	2.6
DR 21 (OH)	39 (0.2)	5.4 (0.1)	34 (1)	5.2 (0.3)	4.5
S 140	26 (1)	2.8 (0.2)	29 (3)	2.6 (0.5)	4.5
Cep A	33 (1)	4.6 (0.4)	53 (18)	5.2 (2.8)	5.7
23033+5951	<34 (7)	< 1.5 (0.5)			
NGC 7538	31 (1)	1.5 (0.1)	32 (13)	1.0 (0.7)	1.9
NGC 7538S	34 (1)	4.6 (0.3)	37 (5)	3.8 (0.8)	5.2

S 140 (Kuiper et al. 1984), and with the abundance, which can be estimated for the cold cloud TMC-1 from the observations of  $\text{C}^{18}\text{O}$  and methyl acetylene (Pratap et al. 1997).

### 3.4. SIMULATIONS OF CHEMICAL EVOLUTION

Using the derived gas temperatures and densities we modelled the chemical evolution of the mapped objects. The chemical reaction network corresponded to the so-called "new standard model" (Lee et al. (1996)). The code for

the simulations was kindly presented by R. Terzieva from Prof. Herbst's group in the Ohio University. The model took into consideration only gas-phase chemistry without any account for dust grains. The initial set of chemical elements corresponded to the low metal abundance (Lee et al. 1996) and is presented in Table 5. The simulations were performed for two C/O ratios, 0.41 and 0.8. The results for NGC 2264 are shown in Fig. 8; the results for other sources are similar. For C/O = 0.41 the  $\text{CH}_3\text{CCH}$  abundance reaches its maximum at  $t_m \approx 6 \times 10^4$  years since the beginning of the evolution; later the abundance decreases

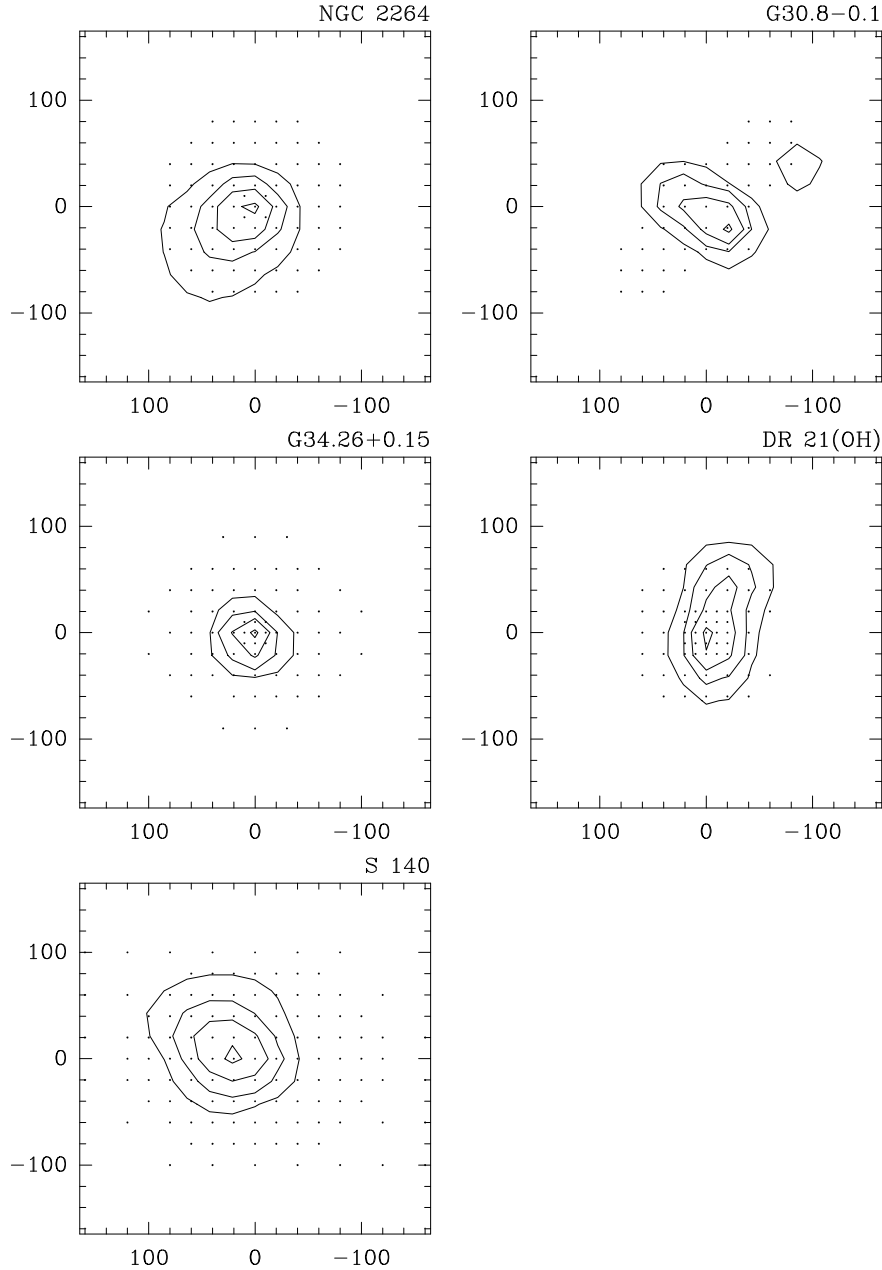


**Fig. 7.** Images of five sources reconstructed by the method of maximum entropy. X and Y axes plot, respectively, the RA and DEC offsets in arcsec from the central positions presented in Table 1. The observed positions are marked by dots.

by several orders of magnitude and reaches steady-state at  $t \geq 10^7$  years. When  $C/O$  increases to 0.8, both  $t_m$  and the maximum  $\text{CH}_3\text{CCH}$  abundance decreases. The comparison of the observed  $\text{CH}_3\text{CCH}$  abundance (Table 3) with the results of our simulations shows that it is the abundance that arises around the peak at  $t_m \approx 6 \times 10^4$  years is characteristic for molecular clouds. The same time dependences are typical for many other molecules (Lee et al.

1996). These results implies a large amount of "chemically young" gas in giant molecular clouds.

Kuiper et al. (1996) in their study of dark clouds considered the model of chemically different shells. In this model, the source consists of a chemically more evolved core, surrounded by a less evolved shell with high abundances of  $\text{CH}_3\text{CCH}$  and other molecules. Such differentiation can be caused by the accretion of rarefied gas. Chemical processes in rarefied gas proceed much more

**Table 4.** Parameters of the mapped sources. Column 1, source; column 2, distance; column 3, angular diameter; column 4, linear diameter; column 5, virial mass; column 6, mass, derived from  $^{13}\text{CO}$  observations; column 7, density, estimated from virial mass; column 8,  $\text{CH}_3\text{CCH}$  abundance, estimated from virial mass and  $\text{CH}_3\text{CCH}$  column density.

Source	d (kpc)	$\Theta$ (")	D (cm)	$M_{\text{vir}}$ ( $M_{\odot}$ )	$M_{\text{CO}}$ ( $M_{\odot}$ )	$n_{\text{H}_2}$ $\text{cm}^{-3}$	$\text{CH}_3\text{CCH}$ abundance
NGC 2264	0.7	57	$6.0 \cdot 10^{17}$	89	40	$4.8 \cdot 10^5$	$1.6 \cdot 10^{-9}$
G30.8-0.1 <sup>1</sup>	6.3	53	$5.0 \cdot 10^{18}$	6208	4919	$5.6 \cdot 10^4$	$4.7 \cdot 10^{-9}$
G34.26+0.15	3.8	42	$2.4 \cdot 10^{18}$	2332	528	$1.9 \cdot 10^5$	$3.6 \cdot 10^{-9}$
DR 21 (OH) <sup>1</sup>	3.0	56	$2.5 \cdot 10^{18}$	1336	1941	$9.6 \cdot 10^4$	$7.7 \cdot 10^{-9}$
S 140	0.9	49	$3.6 \cdot 10^{17}$	135	67	$5.5 \cdot 10^5$	$2.1 \cdot 10^{-9}$

<sup>1</sup>–Unreliable parameters (see sect. "The mapping technique").

**Table 5.** Low-metal initial abundances of chemical elements relative to hydrogen ( $\text{H}_2$ ).

Element	C/O=0.41	C/O=0.8
He	$1.4000 \cdot 10^{-1}$	$1.4000 \cdot 10^{-1}$
N	$2.1400 \cdot 10^{-5}$	$2.1400 \cdot 10^{-5}$
O	$1.7600 \cdot 10^{-4}$	$1.7600 \cdot 10^{-4}$
$\text{C}^+$	$7.3000 \cdot 10^{-5}$	$1.4080 \cdot 10^{-4}$
$\text{S}^+$	$8.0000 \cdot 10^{-8}$	$8.0000 \cdot 10^{-8}$
$\text{Si}^+$	$8.0000 \cdot 10^{-9}$	$8.0000 \cdot 10^{-9}$
$\text{Fe}^+$	$3.0000 \cdot 10^{-9}$	$3.0000 \cdot 10^{-9}$
$\text{Na}^+$	$2.0000 \cdot 10^{-9}$	$2.0000 \cdot 10^{-9}$
$\text{Mg}^+$	$7.0000 \cdot 10^{-9}$	$7.0000 \cdot 10^{-9}$
e	$7.3107 \cdot 10^{-5}$	$7.3107 \cdot 10^{-5}$
$\text{P}^+$	$3.0000 \cdot 10^{-9}$	$3.0000 \cdot 10^{-9}$
$\text{Cl}^+$	$4.0000 \cdot 10^{-9}$	$4.0000 \cdot 10^{-9}$

slowly than in the core; in addition, ultraviolet radiation quickly destroys the formed molecules. Due to a stable influx of "chemically young" substance the shell chemical composition is characterized by high abundances of  $\text{CH}_3\text{CCH}$  and other molecules. However, in neither of the mapped sources could we find any sign of a shell structure. Apparently, this model is not applicable to warm clouds. Note, however, that in all sources, except NGC 2264, we could merely not detect the shell structure because of insufficient spatial resolution.

Another possible explanation of such "chemical" age lie in the fact that during a time of  $\approx 10^5$  years luminous stars may form in the cloud cores. Radiation of these stars leads to the dissipation of the cores. One more explanation is the fact that some processes (e.g., eddy diffusion) may increase the C and  $\text{C}^+$  abundances in the clouds at late stages of their evolution, which in turn increases abundances of different molecules. The review of these and some other possibilities is presented by Bergin et al. (1997).

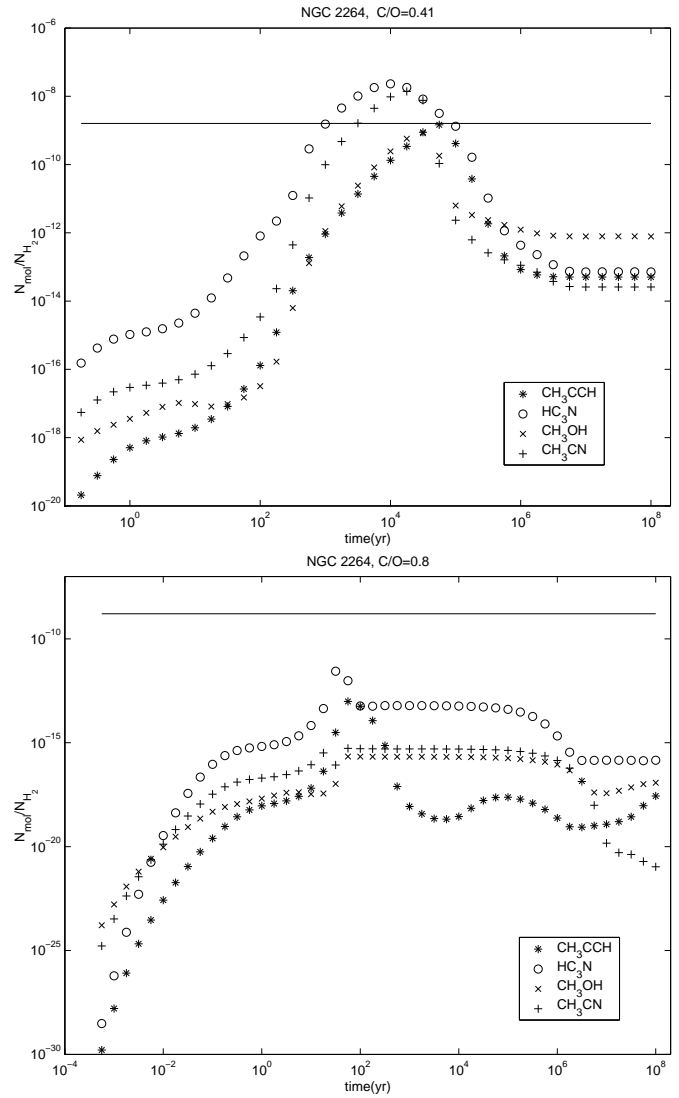


**Fig. 8.** The results of chemical simulations for NGC 2264.

## 4. CONCLUSIONS

As a result of a survey of Galactic star-forming regions in the methyl acetylene lines  $6_K-5_K$  at 102 GHz and  $5_K-4_K$

at 85 GHz, we have detected 44 sources at 102 GHz and 25 sources at 85 GHz.

Using rotational diagrams, we estimated the gas kinetic temperatures and methyl acetylene abundances. The kinetic temperatures appeared to be of the order of 20 – 60 K and coincide within errors with the temperatures that had been estimated from the observations of methanol, methyl acetylene, and ammonia. In most sources methyl acetylene column densities lie in the range  $1 - 5 \times 10^{14} \text{ cm}^{-3}$ . The emission of hot cores, compact massive regions with gas temperatures above 100 K, was not found.

Using the maximum entropy images of five sources, we estimated their sizes, masses, and densities. The sizes proved to be about 0.1 – 1 pc, the masses — hundreds and thousands  $M_{\odot}$ , and the densities — about  $10^5 \text{ cm}^{-3}$ .

Thus, in the lines of methyl acetylene we observed warm and dense clouds.

Simulations of chemical evolution show that the characteristic methyl acetylene abundances in these clouds corresponds to the gas chemical age  $\approx 6 \times 10^4$  years.

#### ACKNOWLEDGMENTS

The authors are grateful to the Onsala Observatory staff for help during the observations, R. Terzieva, who made available the code for the simulations of the chemical evolution of molecular clouds, and Dr. V.I. Slysh for helpful discussion. The work was partially supported by the Russian Foundation for Basic Research (grants no. 98-02-16916 and 01-02-16902), project no. 315 "Radio Astronomy Educational and Scientific Center, and the INTAS grant no. 97-11451. The Onsala Space Observatory is the Swedish National Facility for Radio Astronomy, and is operated by the Chalmers University of Technology, Göteborg, Sweden, with financial support from the Swedish Natural Science Research Council and the Swedish Board for Technical Development.

#### References

- Olmi, L., Cesaroni, R., Neri, R., Walmsley, C. M. 1996, *A&A*, 315, 565
- Kalenskii, S. V., Dzura, A. M., Booth, R. S., Winnberg, A., Alakoz, A. V. 1997, *A&A*, 321, 311
- Wang, T. Y., Wouterloot, J. G. A., Wilson, T. L. 1993, *A&A*, 277, 205
- Bauer, A., Boucher, D., Burie, J., Demaison, J., Dubrulle, A. 1979, *JPCRD*, 8, 537
- Askne, J., Höglund, B., Hjalmarson, Å., Irvine, W. M. 1984, *A&A*, 130, 311
- Kalenskii, S. V., Promislov, V. G., Alakoz, A. V., Winnberg, A., Johansson, L. E. B. 2000, *AZh*, 77, 819
- Mauersberger, R., Henkel, C., Wilson, T. L., Walmsley, C. M. 1986, *A&A*, 162, 199
- Churchwell, E., Walmsley, C. M., Cesaroni, R. 1990, *A&AS*, 83, 119
- Molinari, S., Brand, J., Cesaroni, R., Palla, F. 1996, *A&A*, 308, 573
- Wouterloot, J. G. A., Walmsley, C. M., Henkel, C. 1988, *A&A*, 203, 367
- Schreyer, K., Henning, T., Kömpe, C., Harjunpää, P. 1996, *A&A*, 306, 267
- Wilson, T. L., Mauersberger, R. 1990, *A&A*, 239, 305
- Lucas, R. L., Liszt, H. 1998, *A&A*, 337, 246
- Wilczek, R., Drapatz, S. 1985, *A&A*, 142, 9
- Promislov, V. G., Maximum entropy image restoration by evolutionary algorithm, 1999, *Advances in Soft Computing — Engineering Design and Manufacturing*, Springer – Verlag, London
- Sargent, A. I., Van Duinen, R. J., Nordh, H. L., Fridlund, C. V. M., Aalders, J. W. G., and Beintema D. 1984, *A&A*, 135, 377
- Schreyer, K., Helmich, F. P., van Dishoeck, E. F., Henning, Th. 1997, *A&A*, 326, 347
- Benson, J. M., Johnston, K. J. 1984, *ApJ*, 277, 181
- Carral, P., Welch, W. J., Wright, M. C. H. 1987, *RMxAA*, 14, 506
- Padin, S., Sargent, A. I., Mundy L.G., Scoville, N. Z., Woody, D. P., Leighton, R. B., Masson, C. R., Scott, S. L., Seling, T. V., Stapelfeldt, K. R., Terebey, S. 1989, *ApJ*, 337, L45
- Johnston, K. J., Henkel, C., Wilson, T. L. 1989, *ApJ*, 285, L85
- Mangum, J. G., Wootten, A., Mundy, L.G. 1991, *ApJ*, 378, 576
- Evans, N.J., Mundy, L.G., Kutner, M.L., DePoy, D.L. 1989, *ApJ*, 346, 212
- Snell, R. L., Scoville, N. Z., Sanders, D. B., Erickson, N. R. 1984, *A&A*, 315, 565
- Minchin, N. R., White, G. J., Padman, R. 1993, *A&A*, 277, 595
- Minchin, N. R., White, G. J., Ward-Thompson, D. 1995, *A&A*, 301, 894
- Wilner, D. J., Welch, W. J. 1994, *ApJ*, 427, 898
- Cesaroni, R., Churchwell, E., Hofner, P., Walmsley, C. M., Kurtz, S., 1994, *A&A*, 288, 903
- Panagia, N., Walmsley, C. M. 1978, *A&A*, 70, 411
- Brand, L., Blitz, L. 1993, *A&A*, 275, 67
- Little, L. T., Gibb, A. G., Heaton, D. B., Ellison, B. N., Claude, S. M. X. 1994, *MNRAS*, 271, 649
- Blake, G. A., Sutton, E. C., Masson, C. R., Phillips, T. G. 1987, *ApJ*, 315, 621
- Churchwell, E., Hollis, J. M., 1983, *ApJ*, 272, 591
- Kuiper, T. B. H., Rodriguez Kuiper, E. N., Dickinson, D. F., Turner, B. E., Zuckerman, B. 1984, *ApJ*, 276, 211
- Pratap, P., Dickens, J. E., Snell, R. L., Miralles, M. P., Bergin, E. A., Irvine W. M., Schloerb, F. P. 1997, *A&A*, 486, 862
- Lee, H. H., Bettens, R. P. A., Herbst, E. 1996, *ApJS*, 119, 111
- Kuiper, T. B. H., Langer, W. D., Velusamy, T. 1996, *ApJ*, 468, 761
- Bergin, E. A., Goldsmith, P. F., Snell, R. L., Langer, W. D. 1997, *ApJ*, 482, 285